Chinese Chemical Letters 31 (2020) 2795–2798

Contents lists available at ScienceDirect

Chinese Chemical Letters

journal homepage: www.elsevier.com/locate/cclet

Communication

In situ integration of efficient photocatalyst $Cu_{1.8}S/Zn_xCd_{1-x}S$ heterojunction derived from a metal-organic framework

Dongpeng Zhang[a], Pengfei Wang[b,*], Fangyuan Chen[a], Kelei Mu[a], Yi Li[c], Haitao Wang[a], Zhijun Ren[b], Sihui Zhan[a,*]

[a] MOE Key Laboratory of Pollution Processes and Environmental Criteria / Tianjin Key Laboratory of Environmental Remediation and Pollution Control, College of Environmental Science and Engineering, Nankai University, Tianjin 300350, China
[b] School of Energy and Environmental Engineering, Hebei University of Technology, Tianjin 300401, China
[c] Department of Chemistry, Tianjin University, Tianjin 300072, China

ARTICLE INFO

Article history:
Received 28 May 2020
Received in revised form 25 June 2020
Accepted 26 July 2020
Available online 29 July 2020

Keywords:
Co-catalyst
$Cu_{1.8}S/Zn_{0.35}Cd_{0.65}S$
Density functional theory (DFT)
Charge separation and transfer

ABSTRACT

The development of photocatalysts for hydrogen evolution is a promising alternative to industrial hydrogen evolution; however, generation of high active, recyclable, inexpensive heterojunctions are still challenging. Herein, a novel strategy was developed to synthesize non-noble metal co-catalyst/solid solution heterojunctions using metal-organic frameworks (MOFs) as a precursor template. By adjusting the content of MOFs, a series of $Cu_{1.8}S/Zn_xCd_{1-x}S$ heterojunctions were obtained, and the $Cu_{1.8}S(3.7\%)/Zn_{0.35}Cd_{0.65}S$ sample exhibits a maximum hydrogen evolution rate of 14.27 mmol h^{-1} g^{-1} with an apparent quantum yield of 3.7% at 420 nm under visible-light irradiation. Subsequently, the relationship between the heterojunction and photocatalytic activity were investigated by detailed characterizations and density functional theory (DFT) calculations, which reveal that loading $Cu_{1.8}S$ can efficiently extend the light absorption, meanwhile, the electrons can efficiently transfer from $Zn_{0.35}Cd_{0.65}S$ to $Cu_{1.8}S$, thus resulting more photogenerated electrons participating in surface reactions. This result can be valuable inspirations for the exploitation of advanced materials using rationally designed nanostructures for solar energy conversion.

Photocatalytic hydrogen evolution (PHE) from water utilizing solar energy is a promising and green way to solve the global energy and environment crisis [1]. Since this groundbreaking work was first reported in 1972 by Fujishima and Honda [2], various photocatalysts have been developed over the past several decades. However, the practical application of PHE has still been limited due to the low transmission efficiency of photoexcited charges [3]. In order to solve the above problem, semiconductors are usually modified with co-catalysts to extract electrons for H^+ reduction reaction [4], which can facilitate efficient electron-hole separation and transportation, thus improving the activity and stability of the photocatalysts [5].

To date, a variety of co-catalysts have been used in combination with photocatalysts, including noble metals, transition metal sulfides, oxides, and phosphides [6–11]. Generally, most of the co-catalysts are synthesized in a trial-and-error manner, and the characteristics of easy agglomeration of the nanoparticles lead to uneven distribution of the co-catalysts on the photocatalyst [12], which in turn affects the photocatalytic activity. Recent studies reveal that the nature of a material depends not only on its composition but also on its structure [13–15]. And a good structure can provide more active sites for photocatalytic reactions, meanwhile reducing the transport distance of charge carriers [16,17]. In this context, it has become more urgent to improve the structure of the catalyst, which can develop cheaper and more efficient co-catalysts. However, the development of a simple synthesis process to obtain an inexpensive uniform distribution of co-catalyst/photocatalyst heterojunctions with high PHE activity remains challenging.

Metal organic frameworks (MOFs) are a kind of porous crystalline materials in which metal nodes and organic linkers are covalently linked [18]. Compared to conventional semiconductor photocatalysts, MOFs can contribute to fine-tuning and rational design of active photocatalysts at the molecular level [19]. Due to its unique physicochemical properties and structure, MOFs have recently been widely used as a sacrificial precursor for the preparation of complex structures or specific functional materials

* Corresponding authors.
E-mail addresses: pengfeiwang@hebut.edu.cn (P. Wang), sihuizhan@nankai.edu.cn (S. Zhan).

https://doi.org/10.1016/j.cclet.2020.07.046

[20,21], such as hollow structures [22,23], porous carbon materials [24,25], sacrificial templates [26–28]. The resulting derivatives have abundant active sites and dispersed nanoscale subunits, which confers high catalytic activity in the catalytic field. And the MOFs precursor is uniformly mixed with metal ions at the molecular level and converted to a co-catalyst during the formation of photocatalysts, helping to *in situ* uniformly and more closely load the co-catalyst. However, to date, there have been less reports on the development of co-catalyst /semiconductor heterojunctions using MOF as a precursor.

Herein, we report a novel strategy for preparing photocatalytic hydrogen heterojunctions by using MOFs as a precursor template, resulting $Cu_{1.8}S$ acts as a co-catalyst and $Zn_xCd_{1-x}S$ exists as the solid solution photocatalyst. The obtained new catalytic composite material $Cu_{1.8}S/Zn_{0.35}Cd_{0.65}S$ presents excellent photocatalytic activities under visible light illumination in 0.1 mol/L Na_2S and 0.35 mol/L Na_2SO_3 solutions. And the mechanism of the improvement of photocatalytic activity was studied by theoretical and experimental methods. Consequently, this work has achieved the synergistic integration of photocatalytic components and functional heterostructures, providing an idea for creating new efficient solar-hydrogen conversion photocatalysts.

All chemicals are analytically pure and are used without further purification (Text S1 in Supporting information). Detailed information of synthesis of $Cu_{1.8}S/Zn_xCd_{1-x}S$, characterization and density functional theory (DFT) computational methods *etc.* were given in the Texts S2-S8 (Supporting information). Scheme 1 illustrates a three-step procedure for the synthesis of $Cu_{1.8}S/Zn_xCd_{1-x}S$ heterojunctions, in which $Cu_{1.8}S$ acts as a co-catalyst and $Zn_xCd_{1-x}S$ exists as the solid solution. To better study the transformation of MOFs (HKUST-1) in this process, various characterizations were performed, and $Cu_{1.8}S/Zn_{0.35}Cd_{0.65}S$ was chosen as the model due to its optimized activity. Those detailed analysis processes are described in Text S9 (Supporting information).

The phase structures and average crystallite size (Text S10 in Supporting information) of the prepared samples were determined by X-ray diffraction (XRD). Fig. 1a shows the XRD patterns of $Zn_{0.5}Cd_{0.5}S$ and $Cu_{1.8}S(y\%)/Zn_xCd_{1-x}S$ (x = 0.5, 0.45, 0.4, 0.35, 0.25, y = 1, 2, 2.2, 3.7, 4.8) samples, together with the standard diffraction patterns of the cubic phase ZnS (JPCDS No. 77-2100) and hexagonal phase CdS (JPCDS No. 41-1049) [29]. As the amount of MOFs gradually increased, the XRD diffraction peaks of the corresponding samples show significant changes. Firstly, the diffraction peaks of ZnS (111), (220) and (311) gradually weaken, presumably due to the decrease in the proportion of Zn contents, which corresponds well with the results of Inductively Coupled Plasma-Mass Spectrometry (ICP-MS) (Table S2 in Supporting information). And the Zn/Cd ratio of each sample can be obtained by ICP. Therefore, the addition of different amounts of MOFs precursors in the synthesis helps to well regulate the ratio of Zn/Cd in the solid solution, which is convenient to find the optimized catalyst. Furthermore, the Cu contents also were measured by ICP to indicate the changed amount of co-catalyst $Cu_{1.8}S$ in the samples (Table S3 in Supporting information).

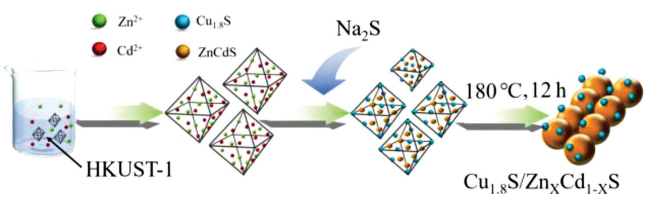

Scheme 1. Schematic illustration of the synthetic procedure for $Cu_{1.8}S/Zn_xCd_{1-x}S$.

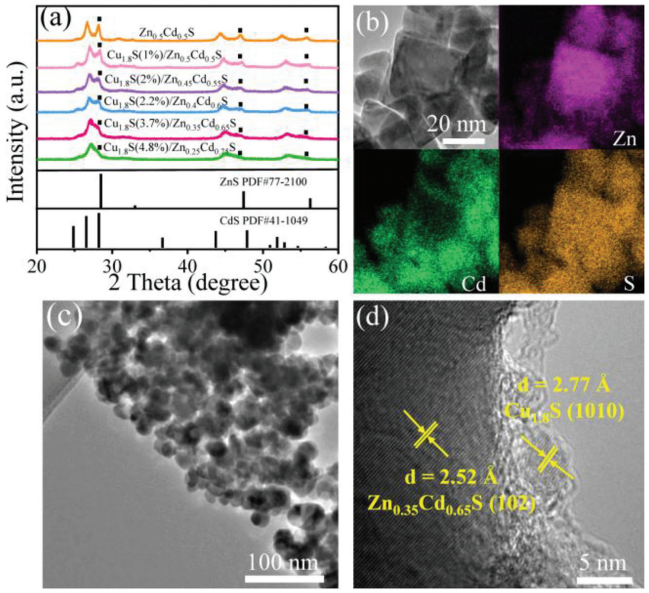

Fig. 1. (a) XRD patterns of the $Cu_{1.8}S(y\%)/Zn_xCd_{1-x}S$ samples. The x and y values were determined by ICP. (b) TEM and elemental mapping images of $Zn_{0.35}Cd_{0.65}S$. TEM (c) and HRTEM (d) images of $Cu_{1.8}S/Zn_{0.35}Cd_{0.65}S$.

As revealed by the images of transmission electron microscopy (TEM) and scanning electron microscopy (SEM) (Fig. 1b and Fig. S3 in Supporting information), the $Zn_{0.35}Cd_{0.65}S$ nanoparticles with single particle size about 20−50 nm. Moreover, we can clearly observe the uniform distribution of the Zn, Cd and S elements in the element mapping image (Fig. 1b), which further indicates the formation of $Zn_{0.35}Cd_{0.65}S$ solid solution [30]. Furthermore, the lattice spacing of 0.325 nm can correspond to the (111) plane of $Zn_{0.35}Cd_{0.65}S$ solid solution in the high resolution TEM (HRTEM) image (Fig. S4 in Supporting information) [5]. For the heterojunctions, the particle size remains about 20−50 nm (Fig. 1c). And the lattice spacings of 0.257 and 0.277 nm can be indexed to the (1010) plane of $Cu_{1.8}S$ and (102) hexagonal plane of $Zn_{0.35}Cd_{0.65}$ solid solutions, respectively (Fig. 1d). $Cu_{1.8}S$ and $Zn_{0.35}Cd_{0.65}$ nanoparticles intimately connect with each other, indicating the formation of heterojunctions, which is advantageous to providing a fast transmission route for photoexcited charge [31]. X-ray photoelectron spectra (XPS) of the hybrid catalyst have been recorded to determine the chemical composition and valence states of the elements in $Zn_{0.35}Cd_{0.65}S$ and $Cu_{1.8}S/Zn_{0.35}Cd_{0.65}S$ (Text S11 in Supporting information). Meanwhile, the formation of heterojunctions also can be confirmed by Raman spectra (Text S12 in Supporting information). Compared to $Zn_{0.35}Cd_{0.65}S$, an additional peak at 4657 cm^{-1} was detected in $Cu_{1.8}S/Zn_{0.35}Cd_{0.65}S$ due to the generation of $Cu_{1.8}S$. Based on the above analysis results, we can conclude that we have successfully prepared a hybrid catalyst based on $Zn_{0.35}Cd_{0.65}S$ solid solution with $Cu_{1.8}S$ as a co-catalyst.

The activity of $Cu_{1.8}S/Zn_xCd_{1-x}S$ is gradually improved when the amount of deposited $Cu_{1.8}S$ is increased (Text S13 in Supporting information), and the maximum H_2 evolution rate of 14.27 mmol h^{-1} g^{-1} is achieved by $Cu_{1.8}S/Zn_{0.35}Cd_{0.65}S$ with 3.7% Cu (wt%) (Fig. 2a). However, further loading of $Cu_{1.8}S$ results in obvious decrease the photocatalytic activity. This is due to the following reasons: (1) As the MOFs (HKUST-1) content added during the preparation increased, the change of Zn/Cd ratio in the prepared sample caused the photocatalytic activity of the catalyst to decrease. (2) $Cu_{1.8}S$ at high loading amount can cover the surface active sites of $Zn_xCd_{1-x}S$ thereby reducing the ability of light absorption and photogenerated charge, causing a "shielding

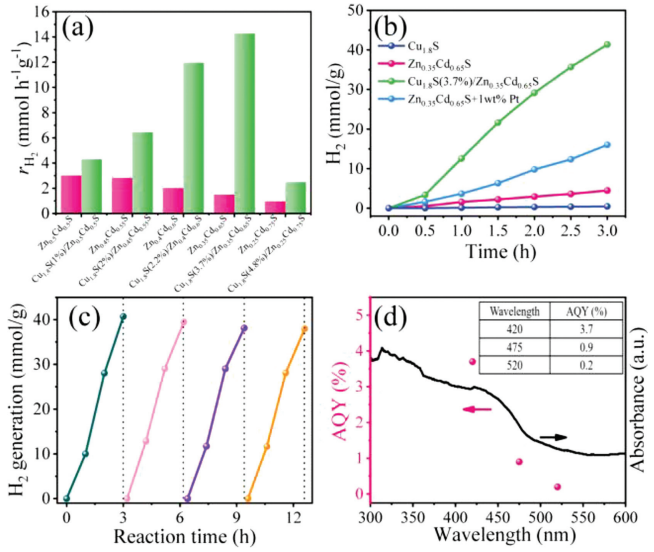

Fig. 2. (a) The rate of hydrogen production of different samples. (b) Photocatalytic hydrogen production profile comparison of the $Cu_{1.8}S/Zn_{0.35}Cd_{0.65}S$ with $Cu_{1.8}S$, $Zn_{0.35}Cd_{0.65}$ and Pt (1 wt%) loaded $Zn_{0.35}Cd_{0.65}S$, the stability study (c) and apparent quantum yield (d) of $Cu_{1.8}S/Zn_{0.35}Cd_{0.65}S$.

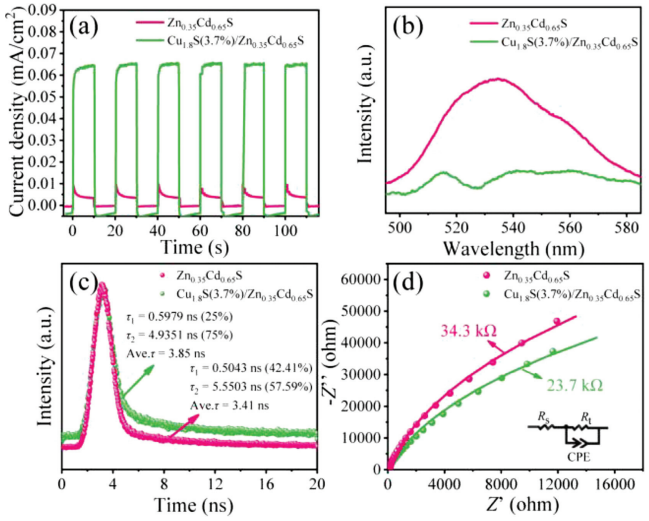

Fig. 3. Transient photocurrent responses (a), steady-state PL spectra (b), time-resolved PL decay spectra of $Zn_{0.35}Cd_{0.65}S$ and $Cu_{1.8}S/Zn_{0.35}Cd_{0.65}S$ (c). (d) Electrochemical impedance spectroscopy (EIS) Nyquist plots of $Zn_{0.35}Cd_{0.65}S$ and $Cu_{1.8}S/Zn_{0.35}Cd_{0.65}S$ in dark.

effect". As shown in Fig. 2b and Fig. S8 (Supporting information), $Cu_{1.8}S/Zn_{0.35}Cd_{0.65}S$ has the best photocatalytic activity of 41.4 mmol g^{-1} in 3 h, which is 9.26 times higher than that of $Zn_{0.35}Cd_{0.65}S$ solid solution (4.47 mmol/g), and even much higher than that of a Pt (1 wt%) loaded $Zn_{0.35}Cd_{0.65}S$ photocatalyst (16.02 mmol/g). In contrast, both $Zn_{0.35}Cd_{0.65}S$ and $Cu_{1.8}S$ exhibit low visible-light hydrogen production activities (Text S14 in Supporting information), indicating that the combination of $Cu_{1.8}S$ and $Zn_{0.35}Cd_{0.65}S$ contributes to charge separation and transfer to enhance photocatalytic activity.

The stability of $Cu_{1.8}S/Zn_{0.35}Cd_{0.65}S$ was tested by repeating the experiments under identical conditions and measuring the hydrogen production rate for each cycle, as shown in Fig. 2c. After 12 h of irradiation without the recovery of catalysts and reagents, $Cu_{1.8}S/Zn_{0.35}Cd_{0.65}S$ is no obvious loss of the photocatalytic hydrogen production activity. In addition, there was no significant change in XRD (Fig. S12 in Supporting information) of $Cu_{1.8}S/Zn_{0.35}Cd_{0.65}S$ before and after the photocatalytic reaction, implying the good stability in a photocatalytic reaction. The apparent quantum yield (AQY) of the $Cu_{1.8}S/Zn_{0.35}Cd_{0.65}S$ photocatalyst was measured at 420, 475, 520 nm by using different band-pass filters (Fig. 2d). The trend in AQY closely follows that of the absorbance measured by ultraviolet-visible spectroscopy, and a relatively high AQY of 3.7% at 420 nm is obtained. As shown in Table S4 (Supporting information), the activity of $Cu_{1.8}S/Zn_{0.35}Cd_{0.65}S$ is compared with other previously reported co-catalyst/solid solution heterojunction catalysts, and the catalyst in this work shows a comparable or higher photocatalytic hydrogen evolution property.

In order to find out the inherent mechanism of the enhanced photocatalytic hydrogen production activity of $Cu_{1.8}S/Zn_{0.35}Cd_{0.65}S$, a series of experiments were conducted. Fig. 3a shows the transient photocurrent response of the samples, and $Cu_{1.8}S/Zn_{0.35}Cd_{0.65}S$ indicates obviously higher response (15.3 times) than that of $Zn_{0.35}Cd_{0.65}S$. This result indicates that $Cu_{1.8}S$ as a high-efficiency co-catalyst makes the separation efficiency of electrons and holes in $Cu_{1.8}S/Zn_{0.35}Cd_{0.65}S$ [32], which might be the reason for the improvement of the photocatalytic activity [33]. Furthermore, the charge separation behavior between $Zn_{0.35}Cd_{0.65}S$ and $Cu_{1.8}S$ was further confirmed by the steady-state photoluminescence (PL) spectra. As shown in Fig. 3b, the emission peak of $Cu_{1.8}S/Zn_{0.35}Cd_{0.65}S$ is significantly weakened in comparison with that of $Zn_{0.35}Cd_{0.65}S$, suggesting the obviously suppressed charge recombination and the faster interfacial charge transfer [34]. In photocatalytic reactions, the longer the lifetime of the charge carrier, the more likely it is to participate in the photocatalytic reaction process [35]. As shown in Fig. 3c, the average PL lifetime of the $Zn_{0.35}Cd_{0.65}S$ and $Cu_{1.8}S/Zn_{0.35}Cd_{0.65}S$ were determined to be 3.41 ns and 3.85 ns, respectively. The elevated PL lifetime confirmed that loading $Cu_{1.8}S$ co-catalysts can facilitate the charge dynamics and elongate the lifetime of charge carriers [36]. Moreover, in order to obtain a deep insight into the charge transport behavior without photoexcitation, EIS measurements were performed under dark conditions (Text S15 in Supporting information). $Cu_{1.8}S/Zn_{0.35}Cd_{0.65}S$ shows a much smaller semicircle diameter and a much lower R_t value than $Zn_{0.35}Cd_{0.65}S$ (Fig. 3d), suggesting its lower interfacial charge-transfer resistance [37].

To gain further insight into the charge separation mechanism of $Cu_{1.8}S/Zn_{0.35}Cd_{0.65}S$, Mott-Schottky measurement and DFT calculations were carried out. Mott-Schottky measurement was used to retrieve quantitative insight about the photoinduced electron density of $Cu_{1.8}S/Zn_{0.35}Cd_{0.65}S$. As is shown in Fig. 4a, both the samples show positive slopes, suggesting they are n-type semiconductors with electrons as major carriers. The linear parts of the plots are extrapolated to $1/C^2 = 0$, the values of E_{fb} are obtained to be −0.47 eV and −0.41 eV for $Zn_{0.35}Cd_{0.65}S$ and $Cu_{1.8}S/Zn_{0.35}Cd_{0.65}S$, respectively. Then, the calculated carrier densities of $Zn_{0.35}Cd_{0.65}S$ and $Cu_{1.8}S/Zn_{0.35}Cd_{0.65}S$ are 1.62×10^{30} cm^{-3} and 7.58×10^{30} cm^{-3} (Text S16 in Supporting information), respectively, suggesting a much faster carrier transfer in $Cu_{1.8}S/Zn_{0.35}Cd_{0.65}S$. Moreover, DFT calculations are used to better understand the carrier transfer process at the interface. As can be seen from Figs. 4b and c, simulated charge distribution show that Cu atoms in $Cu_{1.8}S$ gain electrons (light-blue cloud), meanwhile, Cd atoms and Zn atoms in $Zn_{0.35}Cd_{0.65}S$ lose electrons. Furthermore, the plot vibration of $Zn_{0.35}Cd_{0.65}S$ indicates the charge migrates from $Zn_{0.35}Cd_{0.65}S$ to $Cu_{1.8}S$, and finally achieve a balance (Fig. 4d). All above analysis provide intuitive evidence of charge transfer from $Zn_{0.35}Cd_{0.65}S$ to $Cu_{1.8}S$, resulting more efficient charge separation and more electrons participate in the reduction of H^+. And the Brunauer-Emmett-Teller (BET) test indicates that the change in specific

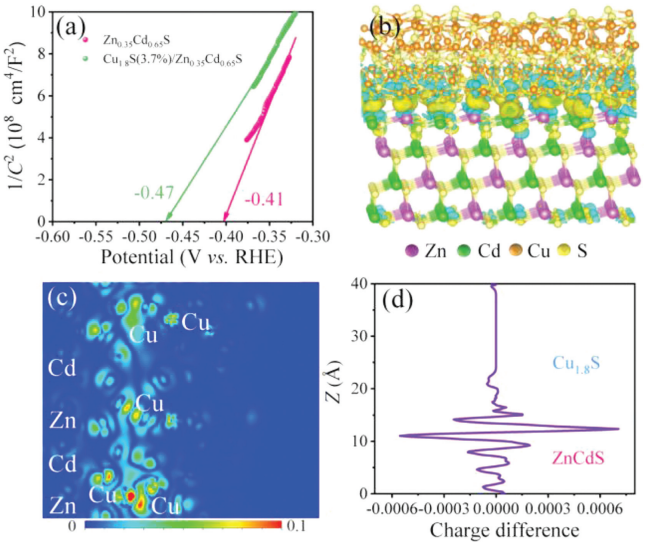

Fig. 4. (a) Mott-Schottky plots of $Zn_{0.35}Cd_{0.65}S$ and $Cu_{1.8}S/Zn_{0.35}Cd_{0.65}S$. (b) Simulated charge distributions at the interface of $Cu_{1.8}S/Zn_{0.35}Cd_{0.65}S$. (c) The planar average charge difference plot as a function of Z coordinate and (d) 2D atomic plane of electron difference density analysis for $Cu_{1.8}S/Zn_{0.35}Cd_{0.65}S$.

surface area is not the main reason for the increase in catalyst activity (Text S17 in Supporting information). To further discuss the mechanism of catalyst activity enhancement, we tested the light absorption capability of samples. The UV–vis absorption spectra of $Zn_{0.35}Cd_{0.65}S$ and $Cu_{1.8}S/Zn_{0.35}Cd_{0.65}S$ are presented in Fig. S15a (Supporting information), which suggest that the adsorption edges of $Zn_{0.35}Cd_{0.65}S$ and $Cu_{1.8}S/Zn_{0.35}Cd_{0.65}S$ are 527 nm and 633 nm, respectively. The detailed analysis processes are described in Text S18 in Supporting information.

Based on above mentioned results, the photocatalytic mechanism is tentatively proposed and illustrated in Fig. S18 (Supporting information). Firstly, loading $Cu_{1.8}S$ on $Zn_{0.35}Cd_{0.65}S$ can extend the light absorption region to the visible region, which facilitates the generation of photoexcited electrons. Secondly, as a co-catalyst, $Cu_{1.8}S$ can effectively capture light-induced electrons form conduction band (CB) of $Zn_{0.35}Cd_{0.65}S$, thereby promoting the transfer of photogenerated electrons. Finally, the electrons could effectively reduce H_2O to produce H_2, and the holes are eliminated by the sacrificial agent (Na_2S/Na_2SO_3). In addition, by using MOFs as a precursor during the preparation process, uniform loading of the co-catalyst *in situ* on the solid solution can increase the number of active sites on the surface. Thus, by virtue of the above advantages, the $Cu_{1.8}S/Zn_{0.35}Cd_{0.65}S$ is endowed with remarkable properties toward photocatalytic hydrogen production.

In summary, a novel strategy for the preparation of $Cu_{1.8}S/Zn_{0.35}Cd_{0.65}S$ heterojunctions for photocatalytic hydrogen production using MOFs as a precursor template was successfully developed. $Cu_{1.8}S(3.7\%)/Zn_{0.35}Cd_{0.65}S$ exhibits a best H_2 production rate of 14.27 mmol h^{-1} g^{-1} under visible light illumination and a high AQY of 3.7% at 420 nm. In addition, experimental characterizations and calculations demonstrate that the increase in hydrogen production activity is due to the efficient separation of charge by $Cu_{1.8}S$ as a highly efficient co-catalyst. This work not only presents a facile method to synthesize highly active $Cu_{1.8}S/Zn_{0.35}Cd_{0.65}S$ for photocatalytic hydrogen, but also provides significant guidance to the rational design and development of novel visible-light-responsive photocatalysts for highly efficient energy conversion.

Declaration of competing interest

The authors declare no conflict of interest.

Acknowledgements

The authors gratefully acknowledge the financially support by the National Natural Science Foundation of China as general projects (Nos. 21722702 and 21874099), the Tianjin Commission of Science and Technology as key technologies R&D projects (Nos. 18YFZCSF00730, 18YFZCSF00770 and 18ZXSZSF00230), National Key Basic Research Program of China (No. 2017YFA0403402), Science and Technology Research Projects of Colleges and Universities in Hebei province (No. ZD2020149).

Appendix A. Supplementary data

Supplementary material related to this article can be found, in the online version, at doi:https://doi.org/10.1016/j.cclet.2020.07.046.

References

[1] S. Chu, A. Majumdar, Nature 488 (2012) 294–303.
[2] A. Fujishima, K. Honda, Nature 238 (1972) 37–38.
[3] K. Wu, Z. Chen, H. Lv, et al., J. Am. Chem. Soc. 136 (2014) 7708–7716.
[4] Y.P. Yuan, L.W. Ruan, J. Barber, S.C. Joachim Loo, C. Xue, Energy Environ. Sci. 7 (2014) 3934–3951.
[5] J. Song, H. Zhao, R. Sun, X. Li, D. Sun, Energy Environ. Sci. 10 (2017) 225–235.
[6] M. Murdoch, G.I.N. Waterhouse, M.A. Nadeem, et al., Nat. Chem. 3 (2011) 489–492.
[7] S. Cao, Y. Chen, C.J. Wang, X.J. Lv, W.F. Fu, Chem. Commun. 51 (2015) 8708–8711.
[8] S.R. Lingampalli, U.K. Gautam, C.N.R. Rao, Energy Environ. Sci. 6 (2013) 3589–3594.
[9] Z. Sun, Q. Yue, J. Li, et al., J. Mater. Chem. A 3 (2015) 10243–10247.
[10] F.N. Sayed, O.D. Jayakumar, R. Sasikala, et al., J. Phys. Chem. C 116 (2012) 12462–12467.
[11] M. Hara, J. Nunoshige, T. Takata, J.N. Kondo, K. Domen, Chem. Commun. (2003) 3000–3001.
[12] P. Wang, S. Zhan, H. Wang, et al., Appl. Catal. B 230 (2018) 210–219.
[13] C. Li, C. Koenigsmann, W. Ding, et al., J. Am. Chem. Soc. 137 (2015) 1520–1529.
[14] H. Lin, B. Sun, H. Wang, et al., Small 15 (2019) 1804115.
[15] Y. Yu, J. Zhang, X. Wu, W. Zhao, B. Zhang, Angew. Chem. Int. Ed. 51 (2012) 897–900.
[16] J. Zhang, Z. Yu, Z. Gao, et al., Angew. Chem. Int. Ed. 56 (2017) 816–820.
[17] Q. Han, B. Wang, J. Gao, L. Qu, Angew. Chem. Int. Ed. 55 (2016) 10849–10853.
[18] R. Wang, L. Gu, J. Zhou, et al., Adv. Mater. Interfaces 2 (2015) 1500037.
[19] Y. Su, Z. Zhang, H. Liu, Y. Wang, Appl. Catal. B 200 (2017) 448–457.
[20] J.D. Xiao, H.L. Jiang, Small 13 (2017) 1700632.
[21] P. Zhang, S. Wang, B.Y. Guan, X.W. Lou, Energy Environ. Sci. 12 (2019) 164–168.
[22] J. Low, C. Jiang, C. Bei, S. Wageh, A.A. Al-Ghamdi, J. Yu, Small Methods 1 (2017) 1700080.
[23] J. Yang, F. Zhang, H. Lu, et al., Angew. Chem. Int. Ed. 54 (2015) 10889–10893.
[24] X. Wang, Z. Chen, X. Zhao, et al., Angew. Chem. Int. Ed. 57 (2018) 1944–1948.
[25] M. Hu, S. Zhao, S. Liu, et al., Adv. Mater. 30 (2018) 1801878.
[26] Q. Sun, N. Wang, J. Yu, J.C. Yu, Adv Mater. 30 (2018) e1804368.
[27] J. Chen, Z. Shen, S. Lv, et al., J. Mater. Chem. A 6 (2018) 19631–19642.
[28] S. Wang, B.Y. Guan, X. Wang, X.W.D. Lou, J. Am. Chem. Soc. 140 (2018) 15145–15148.
[29] Q. Li, H. Meng, P. Zhou, et al., ACS Catal. 3 (2013) 882–889.
[30] M. Liu, D. Jing, Z. Zhou, L. Guo, Nat. Commun. 4 (2013) 2278.
[31] Y. Chen, S. Zhao, X. Wang, et al., J. Am. Chem. Soc. 138 (2016) 4286–4289.
[32] H. Liang, P. Hua, J. Tang, J. Niu, Chin. Chem. Lett. 30 (2019) 2245–2248.
[33] W. Zhen, X. Ning, B. Yang, et al., Appl. Catal. B 221 (2018) 243–257.
[34] S. Yu, X.B. Fan, X. Wang, et al., Nat. Commun. 9 (2018) 4009.
[35] Y. Wang, X. Liu, J. Liu, et al., Angew. Chem. Int. Ed. 57 (2018) 5765–5771.
[36] D. Yuan, M. Sun, S. Tang, et al., Chin. Chem. Lett. 31 (2020) 547–550.
[37] Z. Zhang, H. Cui, J. Tian, et al., Appl. Catal. B 274 (2020) 119114.